### Title
Interaction of a dual-wavelength laser system with cutaneous blood vessels




### ISBN
978-0-8194-6776-8



### Authors
Majaron, Boris
Milanič, Matija
Nelson, J Stuart



### Publication Date
2007-07-05

### DOI
10.1364/ecbo.2007.6632_10

# Interaction of a dual-wavelength laser system with cutaneous blood vessels

Boris Majaron[*a,b], Matija Milanič[a], J. Stuart Nelson[b,c]
[a]Jožef Stefan Institute, Jamova 39, SI–1000 Ljubljana, Slovenia
[b]Beckman Laser Institute and Medical Clinic, University of California at Irvine
[c]Department of Biomedical Engineering, University of California at Irvine

## ABSTRACT

Our working hypothesis is that a dual-wavelength Nd:YAG laser, emitting simultaneously at 1064 and 532 nm, may induce stronger heating of PWS blood vessels relative to the epidermis than the customary KTP laser, due to conversion of hemoglobin to met-hemoglobin in the target blood vessels and the associated increase in NIR absorption. We apply pulsed photothermal radiometry to determine temperature depth profiles induced in PWS lesions by a dual-wavelength laser at sub-therapeutic radiant exposures. The results indicate no effect at 1 ms pulse duration and low radiant exposures (1–2 J/cm$^2$). Increased radiant exposure (3–4 J/cm$^2$) and extended pulse duration (20–25 ms) result in increased energy deposition. In addition, two PWS lesions and one healthy skin site were irradiated at incrementally increasing radiant exposures, up to 9 J/cm$^2$. Analysis of the laser-induced temperature profiles clearly revealed irreversible changes of tissue properties. Formation of met-hemoglobin and consequent increase of IR absorption was however not reliably detected.

**Keywords:** laser therapy, port wine stain, pulsed photo-thermal radiometry, temperature depth profiling, dual-wavelength laser, met-hemoglobin

## 1. INTRODUCTION

Port wine stain birthmarks (PWS) consist of normal epidermis overlying an abnormal plexus of dilated blood vessels within the most superficial millimeter of the dermis. Depth and size distribution of PWS blood vessels is variable, but on average, the highest fractional blood content is found 0.2–0.4 mm below the epidermal-dermal junction.[1] Laser therapy of PWS currently utilizes selective photocoagulation of blood vessels using pulsed green or yellow lasers. However, non-specific absorption by epidermal melanin reduces the amount of incident radiation that reaches target chromophores - hemoglobin in PWS blood vessels. Moreover, overheating of epidermis can induce blistering, dyspigmentation, or scarring of skin. This limits the radiant exposure that can be safely applied in therapy, thus impairing treatment efficacy in many patients, despite recent implementation of dynamic cooling.[2,3]

Because melanin absorption decreases with increasing wavelength,[4] the hypothesis is that additional irradiation at 1064 nm may help induce a higher temperature rise in PWS vessels relative to the epidermis, as compared to irradiation at 532 nm alone. Moreover, Barton *et al* have recently reported and studied chemical transformations of native hemoglobin species to met-hemoglobin upon laser irradiation at 532 nm,[5,6] which should lead to significant increase of near-IR absorption in blood vessels. From their data, first sings of transformation begin after deposition of ~3–5 J/cm$^2$ (delivered over 3–5 ms). Such effects could play an important role in vascular treatments using near-IR[7,8] and dual-wavelength lasers.[9]

In present study, we measure temperature depth profiles induced in PWS skin in vivo by a dual-wavelength laser system, emitting simultaneously at 1064 nm and 532 nm. By comparing the results with those obtained using a customary KTP/Nd:YAG vascular laser (emitting at 532 nm only) and analyzing the temperature profiles as a function of radiant exposure, we try to demonstrate and characterize formation of met-hemoglobin in PWS in vivo.

[*] boris.majaron@ijs.si; phone: +386 1 477-3208, fax: +386 1 423-5400; http://complex.ijs.si/index.html

Therapeutic Laser Applications and Laser-Tissue Interactions III, edited by Alfred Vogel, Proc. of SPIE-OSA Biomedical Optics, SPIE Vol. 6632, 66320C, © 2007 SPIE-OSA · 1605-7422/07/$18

The laser-induced temperature profiles were measured by means of pulsed photothermal radiometry (PPTR). PPTR is based on time-resolved acquisition of IR emission from the sample surface after pulsed laser exposure. With known optical and thermal properties of the sample, the temperature depth profiles can be reconstructed from acquired transient radiometric signals by solving the inverse problem of heat diffusion and blackbody emission.[10,11] This technique allows depth profiling in optically scattering samples, including biological tissues,[12,13,14] and has been suggested earlier for characterization of PWS lesions.[15,16,17]

## 2. METHODOLOGY

### 2.1 PWS lesion preparation and laser irradiation

Measurement sites involved in this report include two PWS lesion sites on forearms of two volunteer patients (W and K), one on hand (W) and one on face (E). For comparison purposes, we have taken PPTR measurements also on the inner side of a forearm of a volunteer with normal, healthy skin (B). Prior to irradiation, selected areas were shaved (if necessary), and the stratum corneum (thin, dehydrated outer layer of skin) was removed by tape stripping. The remnants of stratum corneum and glue were subsequently washed off using medical grade ethanol. After re-moistening the skin with saline pads and wiping off excess liquid with paper tissue or gauze, the prepared site was positioned against a 1 cm aperture in the object plane of the IR camera optics (see Fig. 1).

The Dualis Tandem laser system prototype (by Fotona, Ljubljana, Slovenia) emits 1–50 ms long pulses at 532 and 1064 nm simultaneously. Approximately 36% of the total pulse energy is emitted at 532 nm, the remaining 64% at 1064 nm. The system has obtained a 510k approval for treatment of vascular lesions from the US Food and Drugs Administration (FDA).

In the first set of presented PPTR measurements, radiant exposure at the skin surface was strictly sub-therapeutic. The 532 nm component amounted to $H_0 = 0.5$ J/cm$^2$ in 1 ms laser pulses, and 1.4 J/cm$^2$ at 25 ms. For comparison measurements, we used a standard KTP/Nd:YAG dermatologic laser system emitting at 532 nm (VersaPulse by Lumenis, Santa Clara, CA). The radiant exposure with 2 ms and 20 ms pulses was 1.9 and 3.2 J/cm$^2$, respectively. In one example, we have employed also a pulsed dye laser (PDL; SPTL1b by Candela, Wayland, MA) with pulse duration of 1.5 ms and radiant exposure of 2.2 J/cm$^2$.

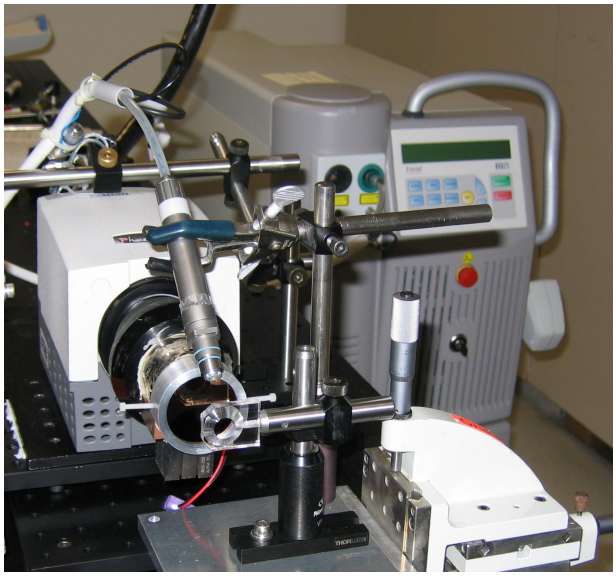

Figure 1: Experimental setup for pulsed photothermal radiometry (PPTR) of human skin. Light pulses from the therapeutic laser system (far right) are delivered to the handpiece (stripped of the plastic casing and cryogen spray nozzle) via an optical fiber. Emitted pulses are directed into the center of a 1 cm aperture which enables accurate positioning of the test site in the object plane of the IR camera's macro objective.

The above radiant exposure values were determined by measuring laser pulse energy transmitted through a 0.72 mm diameter pinhole in the object plane. Lateral scanning of the aperture across the field of view of the IR camera has

verified homogeneity of the radiant exposure. The pyroelectric detector (J25LP-1, Molectron, Portland, OR) was customized by the manufacturer to allow measurements of such relatively long laser pulses.

In the second set of experiments, the green radiant exposure of the dual-wavelength laser was increased incrementally from around 1–2 J/cm$^2$ toward the therapeutic threshold values (6–9 J/cm$^2$), using the laser's control panel. The reported radiant exposure values rely on laser system's self-calibration feature and the ratio between the nominal spot size (instrument setting: 5 mm diameter) and actual area of the laser spot on the irradiated skin. Due to oblique incidence of the laser beam onto the test site (see Fig. 1), the latter is approximately an ellipse with the primary axes ranging from 3.5 by 4 mm (patient E, irradiation at a 30 degree angle) to 4 by 6 mm (volunteer B, irradiation at 45 degrees).

### 2.2 Pulsed photothermal radiometry – basics

Detailed discussion of PPTR depth profiling in semi-infinite media can be found elsewhere.[16,18,19] In short, one-dimensional approximation is valid as long as the laser irradiated spot is much larger than the involved optical penetration depths and thermal diffusion lengths. Planck's law of radiation, which describes the locally emitted power density at wavelength $\lambda$, is linearized around the initial skin temperature, $T_0$: $B_\lambda(T) \approx B_\lambda(T_0) + B_\lambda'(T_0)\,\Delta T$. Due to the finite absorption coefficient of the emitted IR radiation ($\mu_{IR}$), radiometric signal from a non-uniformly heated object is composed of appropriately attenuated contributions from different depths $z$. The radiometric signal $S(t)$ is thus expressed as

$$S(t) \;=\; C\,B_\lambda(T_0) \;+\; C\,B_\lambda'(T_0)\,\mu_{IR}\int_{z=0}^{\infty}\Delta T(z,t)\,e^{-\mu_{IR}z}\,dz\,, \tag{1}$$

where constant $C$ accounts for optical properties of the sample surface and collection optics, and detector specifics. Temperature field evolution in the sample, $\Delta T(z,t)$, is a convolution of the laser-induced temperature rise, $\Delta T(z,t=0)$, and the thermal point-spread function of the sample. Since the latter is known explicitly,[16] convolution with the exponential attenuation function in (1) can be performed, yielding a simple integral expression for the transient part of the radiometric signal, $\Delta S(t)$:

$$\Delta S(t) = \int_{z=0}^{\infty} K(z,t)\,\Delta T(z,0)\,dz\;. \tag{2}$$

In the following, we apply kernel function $K(z,t)$ as derived by Milner *et al.*[16], with thermal diffusivity of skin $D = 1.1 \times 10^{-7}$ m$^2$s$^{-1}$ and reduced heat transfer coefficient at the surface equal to $h = 0.02$ mm$^{-1}$.

### 2.3 Experimental setup

In the first experimental setup, light pulse emitted from the laser handpiece is reflected onto the target skin site by a micro-prism (not shown in Fig. 1). A unity magnification IR optics (f/2) images the central 1.9 × 1.9 mm$^2$ area of the irradiated site onto a liquid-nitrogen cooled InSb focal-plane array (FPA) detector of the IR camera (Galileo, Raytheon, Dallas, TX). By reading out only a 64 × 64 subset of all FPA elements, the signal acquisition rate is 700 frames per second (at 0.9 ms integration time for each frame). The acquired data are digitized with a 12-bit A/D converter and transferred to personal computer's memory.

In the second set of measurements, the transient increase in IR emission is imaged by a macro lens with magnification of 0.5 (patients E and K) or 1 (volunteer B) and recorded with a thermo-electrically cooled InSb IR camera (Phoenix, Indigo, Santa Barbara, CA). By using a 128 × 64 sub-window on the FPA, and detector integration time set to 0.577 ms, we can acquire 1000 IR emission images per second. The transient IR signal is acquired 1–2 s post irradiation and digitized with a 14-bit A/D converter.

Because $\mu_{IR}$ of skin varies by two orders of magnitude within the 3–5 μm detection band of the InSb detector, a custom filter is applied to narrow the acquisition spectral band to 4.5–5.0 μm. In this way, the customary monochromatic approximation applied in subsequent signal analysis adequately represents IR properties of human skin.[19,20,21]

### 2.4 Signal analysis

PPTR signals $\Delta S(t)$ are computed from the recorded IR emission images by calibrating the system response with a computer-controlled blackbody (BB701, Omega Engineering, Stamford, CT), averaging laterally over the FPA subwindow, and subtracting the background signal level. Only one laser pulse needs to be applied for each PPTR measurement. However, in view of the moderate signal-to-noise ratios and severe ill-posednes of the ensuing mathematical analysis, we sometimes average 2–3 experimental signals acquired on the same skin site and under the same conditions.

Finally, the initial temperature profiles $\Delta T(z,0)$ are reconstructed by solving the inverse problem of heat diffusion and blackbody emission. The effective IR absorption coefficient value ($\mu_{IR} = 24.2$ mm$^{-1}$) was calculated from model composition of human skin (75% water, 25% collagen)[22] using a dedicated algorithm,[23] which will be described in detail elsewhere. We apply a conjugate-gradient minimization algorithm with non-negativity constraint, and regularize by early termination via consultation of the so-called L-curve.[16] In analysis of the second measurement set, we solve the minimization problem using a novel optimization algorithm, which combines the minimal-error conjugate gradients scheme with non-negativity constraint and includes automatic adaptive regularization according to discrepancy principle.[20] Reconstruction of temperature profile, represented by 150 values over a depth range of 1.5 mm, is typically accomplished on a personal computer in less than a second.

## 3. RESULTS

### 3.1 Comparison of PWS temperature profiles

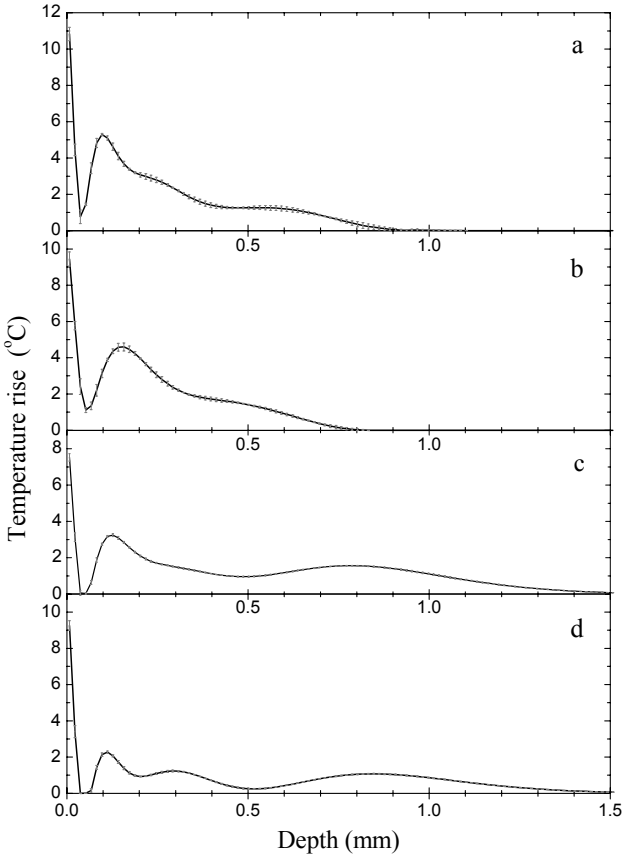


Figure 2: Temperature profiles in PWS lesion on patient's hand (W) after irradiation with:
(a) a standard 532 nm laser at 2 ms pulse duration,
(b) the dual-wavelength Tandem laser at 1 ms,
(c) pulsed dye laser at 585 nm and 1.5 ms,
(d) pulsed dye laser at 600 nm and 1.5 ms.
All temperature profiles are normalized to the visible radiant exposure equal to $H_0 = 1$ J/cm$^2$.

Figure 2 presents reconstructed temperature profiles in PWS lesion on patient's hand (W) after irradiation with a standard 532 nm KTP laser (Fig. 2a), the dual-wavelength laser (Fig. 2b), pulsed dye laser at 585 nm (Fig. 2c), and

pulsed dye laser at 600 nm (Fig. 2b). All pulse durations are between 1 and 2 ms and radiant exposures are between 1.5 and 2.2 J/cm$^2$. For the purpose of comparison, the presented temperature profiles are normalized to the same visible radiant exposure, $H_0$ = 1 J/cm$^2$. The solid lines and error bars represent, respectively, mean values and standard deviations of the temperatures at each depth, as computed from a few near-optimal iterative solutions.

The results indicate little difference between the 532 and dual-wavelength irradiation at the same visible radiant exposure. Pulsed dye laser (PDL) at either wavelength induces less aggressive heating of the superficial PWS layer (0.1–0.3 μm), but has a significant effect deeper than 0.8 mm (and down to 1.5 mm), where the influence of both KTP and Tandem laser is absent. PDL at 600 nm causes weaker heating of PWS than at 585 nm, as expected from both theory and clinical evidence. Perhaps surprisingly, however, the depth of the effect is the same for both PDL wavelengths.

From simple calorimetric reasoning, we can assess surface density of the deposited laser energy converted to heat, $\varepsilon$, from the area under the reconstructed temperature profile:

$$\varepsilon = \rho\, c \int_0^\infty \Delta T(z)\, dz\,. \tag{3}$$

The values, obtained from results in figure 2 using thermal properties of human dermis (mass density $\rho$ = 1150 kg/m$^3$, specific heat capacity $c$ = 3500 J/kgK), are presented in Table 1. The fraction of delivered (visible) radiant exposure deposited as heat is very similar between the dual-wavelength laser (Tandem) and the 532 nm KTP laser. The "missing" fraction amounts to 33–36%, which corresponds to reflectivity of fair skin at 532 nm.[24] The deposition efficiency at 585 nm is slightly higher, likely due to somewhat lower melanin absorption coefficient and dermal scattering coefficient as compared with 532 nm. The significant drop in $\varepsilon$ at 600 nm can be attributed to markedly reduced blood absorption, which results in increased diffuse reflection of skin *in vivo*.[24]

Table 1: Surface density of deposited laser energy ($\varepsilon$) assessed from PWS temperature profiles in figure 2 (patient W, hand) at nominal radiant exposure $H_0$ = 1 J/cm$^2$.

| Laser | KTP | Tandem | pulsed dye | |
|---|---|---|---|---|
| Wavelength [nm] | 532 | 532 + 1064 | 585 | 600 |
| $\varepsilon$ [J/cm$^2$] | 0.67 | 0.64 | 0.72 | 0.47 |

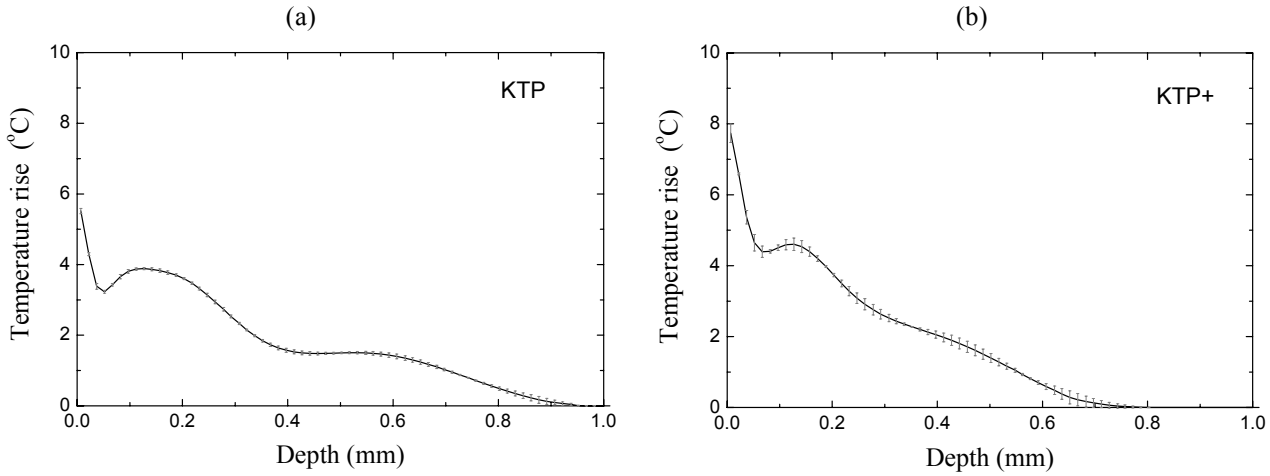


Figure 3: PWS temperature profiles in patient's hand (W) after irradiation with (a) a standard 532 nm laser at pulse duration of 20 ms, and (b) the dual-wavelength laser at 25 ms. Both temperature profiles are normalized to the 532 nm radiant exposure of $H_0$ = 1 J/cm$^2$.

Figure 3 presents temperature profiles induced in the same PWS lesion (patient W, hand) with the 532 nm laser at pulse duration of 20 ms (Fig. 3a) and dual-wavelength laser at 25 ms (Fig. 3b). The respective radiant exposures were 3.2 J/cm$^2$ and 3.9 J/cm$^2$. With both temperature profiles normalized to the 532 nm radiant exposure of $H_0$ = 1 J/cm$^2$, we can see that at these, somewhat higher radiant exposures and longer pulse durations, the dual-wavelength irradiation induces a higher peak temperature rise (4.6 °C) than the usual KTP laser (3.9 °C). The subsurface temperature peak is located a little shallower (120 vs. 130 μm) and the observable temperature rise extends less deep in comparison (approximately 0.7 vs. 0.9 mm), suggesting that absorption in blood is increased upon addition of the 1064 nm radiation. However, the epidermal temperature rise increases by a similar ratio.

Finally, we compare PWS temperature profiles after irradiation with the dual-wavelength laser at pulse durations of 1 ms (lighter lines) and 25 ms (darker lines). The results are presented for the forearm (Fig. 4a) and hand (Fig. 4b) of the same PWS patient (W). All temperature profiles are normalized to the same 532 nm radiant exposure of $H_0$ = 1 J/cm$^2$.

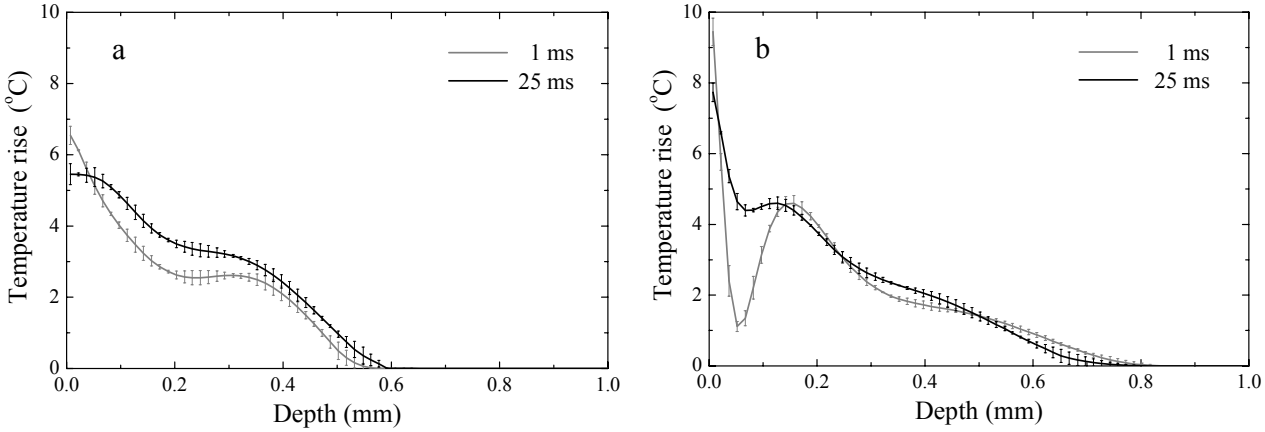


Figure 4: Temperature profiles in PWS on volunteer patient's (a) forearm and (b) hand, immediately after irradiation with the dual-wavelength laser at pulse duration of 1 ms (lighter line) and 25 ms (darker line). All temperature profiles are normalized to the same 532 nm radiant exposure ($H_0$ = 1 J/cm$^2$). The lines and error bars represent, respectively, the mean value and standard deviation of the temperature at each depth, as computed from a few near-optimal iterative solutions according to L-curve analysis.

In both test sites, the temperature profiles induced with the longer pulse duration are smoother and the surface temperature is significantly reduced. The PWS temperature is in general somewhat higher (Fig. 4a) or practically the same (Fig. 4b) as with 1 ms irradiation. However, in both test sites is the associated surface density of deposited laser energy $\varepsilon$ (3) higher with the longer laser pulses and accordingly higher radiant exposure (see Table 2).

Table 2: Surface density of deposited laser energy ($\varepsilon$) assessed from PWS temperature profiles in figure 4 at nominal radiant exposure $H_0$ = 1 J/cm$^2$. (Patient W)

| PWS site | forearm | | hand | |
|---|---|---|---|---|
| pulse duration [ms] | 1 ms | 25 ms | 1 ms | 25 ms |
| $\varepsilon$ [J/cm$^2$] | 0.59 | 0.70 | 0.64 | 0.72 |

### 3.2 Influence of radiant exposure

Figure 5 presents IR emission images acquired 1 ms and 200 ms after irradiation with a 25 ms dual-wavelength laser pulse (Figs. 5a and 5b, respectively). In this example (healthy skin on forearm of volunteer B), the imaged area is $2 \times 4$ mm$^2$. The early image reflects microscopic superficial structure of human skin and non-homogeneous melanin distribution, while the latter is dominated by chromophore distribution in deeper skin layers. The corresponding PPTR signal is computed from the indicated central part of the irradiated site (dashed square, $0.5 \times 0.5$ mm$^2$).

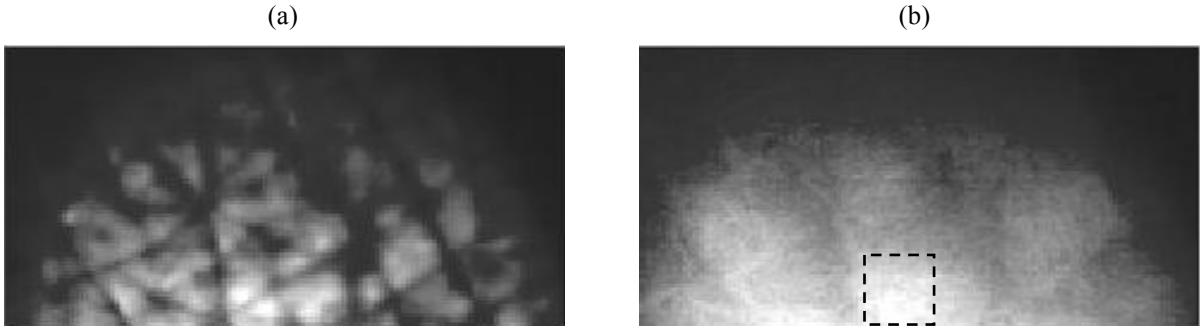


Figure 5: Example IR emission images acquired from healthy skin on forearm (volunteer B), 1 ms (a) and 200 ms (b) after irradiation with a 25 ms dual-wavelength laser pulse. In this example, the imaged area is $2 \times 4$ mm$^2$. The corresponding PPTR signal is computed from the indicated central part of the irradiated site (dashed square, $0.5 \times 0.5$ mm$^2$).

Figure 6a presents PPTR signals acquired from PWS on volunteer patient's (E) face after pulsed irradiation with the dual-wavelength laser and 532 nm radiant exposure $H_0$ increasing in equal increments from 1.8 to 9 J/cm$^2$. PPTR signals in Figure 6b were acquired from the same lesion site and with same laser at $H_0 = 1.8$ J/cm$^2$ and 9 J/cm$^2$, immediately after completion of the previous irradiation sequence (delivering 34 J/cm$^2$ distributed between 8 laser pulses in approximately 5 minutes). The altered signal shape clearly reveals a change in optical properties of some lesion component(s).

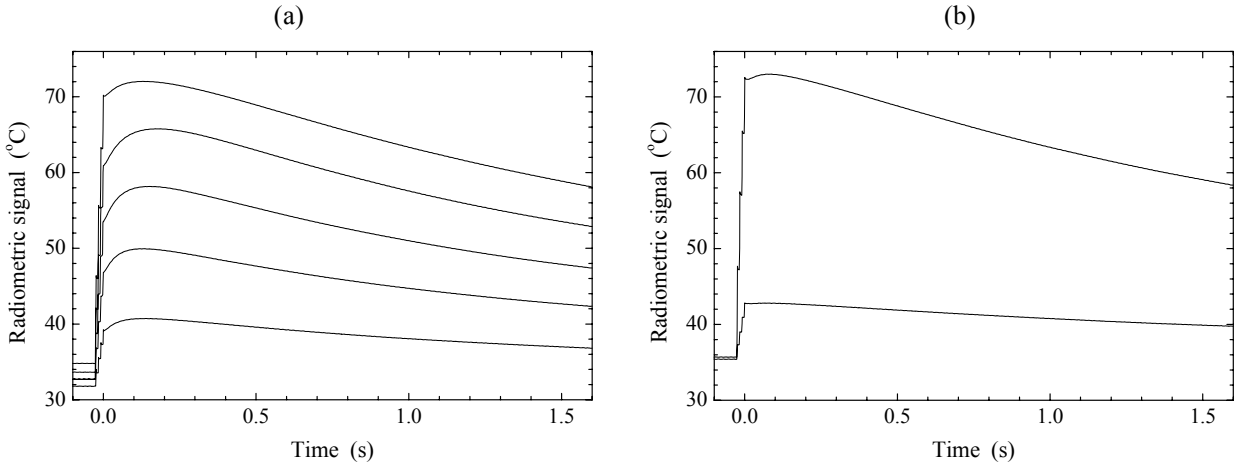


Figure 6: (a) PPTR signals acquired from PWS on volunteer patient's (E) face after pulsed irradiation with the dual-wavelength laser at radiant exposure ($H_0$) of 1.8, 3.6, 5.4, 7.2, and 9.0 J/cm$^2$. (b) PPTR signals acquired from the same lesion site with same laser at $H_0 = 1.8$ J/cm$^2$ and 9.0 J/cm$^2$, after completion of the previous irradiation sequence.

Figure 7 shows PWS temperature profiles reconstructed from the above PPTR measurements. The PWS peak temperature (~0.2 mm below the surface) initially increases in proportion with the radiant exposure, up to 6 J/cm$^2$ (Fig. 7a). At higher radiant exposures, temperature rise at this depth increases sub-linearly with $H_0$ and peak of the PWS temperature profile moves significantly deeper into the lesion. The peak epidermal temperature increases

proportionally with radiant exposure up to $H_0$ = 8 J/cm$^2$. The super-linear increase with the last exposure increment is a plausible consequence of the reduced absorption at 0.1–0.3 mm, which raises the epidermal fluence.

Temperature profile in the same lesion site induced with $H_0$ = 1.8 J/cm$^2$ immediately after completion of the discussed irradiation/measurement sequence (Fig. 7b, solid line) demonstrate that the effects mentioned above – reduced blood absorption at 0.1–0.3 mm with consequent increase in epidermal temperature rise and deeper reach of laser heating - were irreversible.

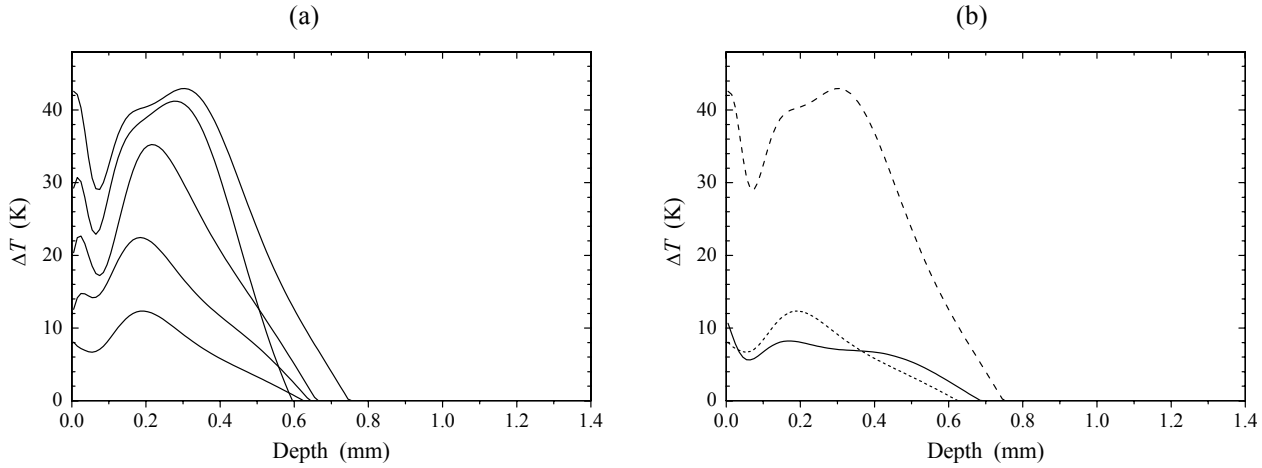


Figure 7: Reconstructed temperature profiles in PWS on volunteer patient's face (E) after pulsed irradiation with the dual-wavelength laser at (a) radiant exposure $H_0$ incrementally increasing from 1.8 to 9.0 J/cm$^2$. (b) Temperature profile in the same lesion site induced with $H_0$ = 1.8 J/cm$^2$ after completion of the previous irradiation/measurement sequence (solid line). Two extreme results from the previous graph are plotted for comparison (dashed lines).

Figure 8 presents temperature profiles obtained form healthy skin site (volunteer B, forearm). After performing PPTR depth profiling with the dual-wavelength laser and radiant exposure increasing from 1 J/cm$^2$ to 5 J/cm$^2$ (in increments of 1 J/cm$^2$ and two measurements at each $H_0$ value), the same measurement sequence was repeated on the same test site in reverse order. The results indicate an irreversible modification at the test site, manifesting itself in slightly reduced surface temperature, increased heating from ~30 μm to 0.5 mm, and reduced heating effect beyond that depth (Fig. 8b, solid lines).

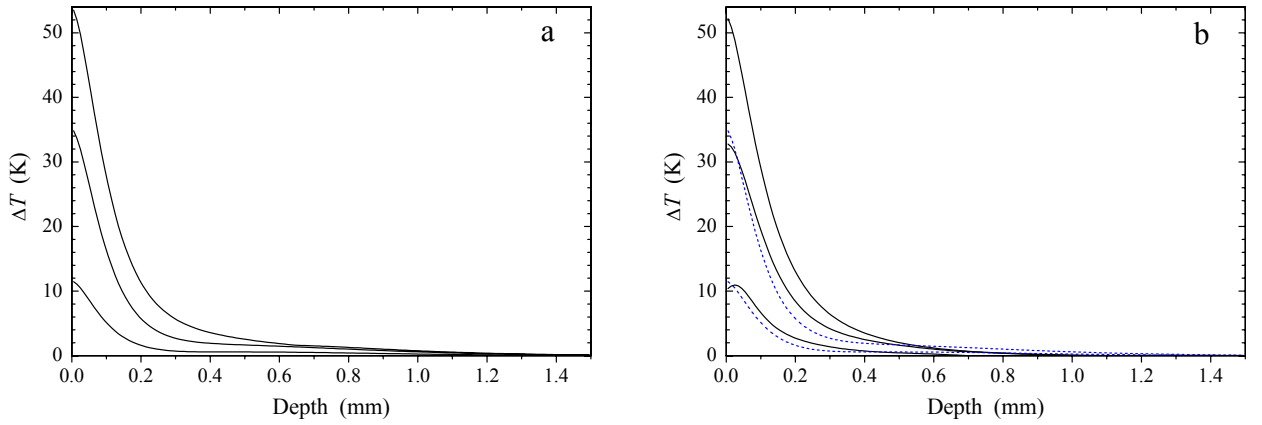


Figure 8: Temperature profiles induced by pulsed irradiation of healthy skin on forearm (volunteer B) with the dual-wavelength laser at (a) radiant exposure $H_0$ of 1, 3, and 5 J/cm$^2$. (b) Temperature profile at the same test location site induced using same radiant exposures after completion of the previous irradiation/measurement sequence (solid lines). Two results from the previous graph are plotted for comparison (dashed lines).

## 4. DISCUSSION

Temperature profiles in Fig. 2 indicate little difference between the temperature profiles induced in PWS lesion with 532 nm or dual-wavelength irradiation at the same visible radiant exposure. This is not so surprising because the applied radiant exposures were very low; 0.5 J/cm$^2$ at 532 nm and 0.9 J/cm$^2$ at 1064 nm delivered in 1 ms pulse from the Tandem laser. Hemoglobin absorption at 1064 nm is namely 100–250 times lower than at 532 nm (assuming 80% oxygen saturation) and conversion to met-hemoglobin reportedly occurs only after deposition of 3–5 J/cm$^2$ of 532 nm light, delivered over 3–5 ms.[5,6] Meanwhile, Nd:YAG lasers for vascular therapy and hair removal typically employ pulse energies approaching 100 J/cm$^2$.

Weak near-IR absorption of both hemoglobin and melanin on one hand leads to high diffuse reflectivity of skin (exceeding 50% at $\lambda = 800$ nm[24]). Accentuated by the low reduced scattering coefficient, it results also in large optical penetration depth at 1064 nm (on the order of mm). We thereby allow that the complete absence of detectable heating due to IR component of the dual-wavelength laser may be in part due to energy deposition at depths out of reach for PPTR profiling, in addition to the high skin reflectivity at 1064 nm.

It is interesting that the pulsed dye laser (PDL) at both 585 and 600 nm wavelength induced a much lesser heating of the superficial, cosmetically relevant PWS layer (depth 0.1–0.3 μm), but caused much deeper heating of the dermal vasculature (Fig. 2). With PDL, heating of skin could be observed up to 1.5 mm deep, while the influence of both KTP and dual-wavelength laser was limited to ~0.8 mm. This difference could result from combined effect of somewhat lower melanin absorption coefficient and reduced scattering coefficient at 585 nm as compared to 532 nm.

The much smaller deposited energy density ($\varepsilon$) at 600 nm as compared to 585 nm (Table 1) can be attributed to markedly reduced blood absorption. This enhances the effect of dermal backscatter and results in significant increase in diffuse reflection in this spectral range.[24] The same effect is responsible also for the larger epidermal temperature rise at 600 nm in comparison with 585 nm (Fig. 2c, 2d), despite the fact that melanin absorption is monotonically decreasing with wavelength.[4] We have observed the same effect in numerical modeling of optical transport in PWS.[25]

Further insight into dynamics of dual-wavelength laser interaction with PWS lesion can be obtained from analysis of temperature profiles induced with incrementally increasing radiant exposure (Figs. 7, 8). As long as optical properties of the lesion are constant, the deposited energy density ε (3) should namely increase proportionally with radiant exposure. Contrariwise, a super-linear relation would reveal presence of additional chromophore (e.g. met-hemoglobin, with 5 times higher absorption at 1064 than hemoglobin).

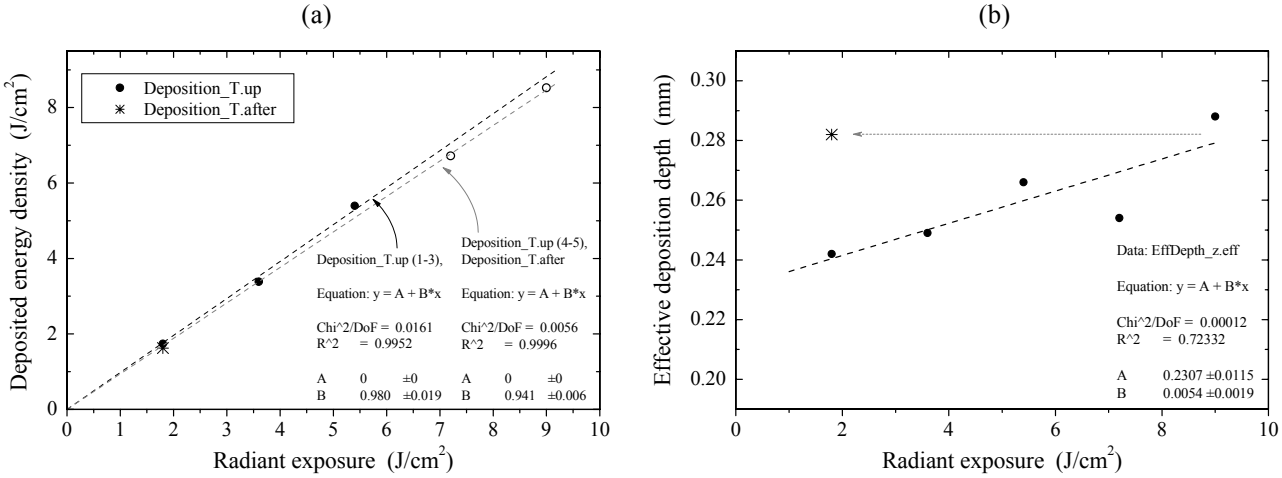


Figure 9: (a) Deposited heat per surface area ε (3), and (b) effective deposition depth ζ (4) in PWS as a function of 532 nm radiant exposure. Dashed lines are linear fits – see text for explanation. (patient E, dual-wavelength irradiation)

The results of such analysis are presented in Figure 9a. Evidently, the values for the two highest radiant exposures (open circles) are not above the straight line fitted to the first three data points (dashed line and solid circles,

respectively). Since the temperature profiles in Figs. 7a and 7b strongly suggest that irreversible modification of optical properties has taken place in the lesion upon exceeding a certain exposure threshold (tentatively around 5–6 J/cm$^2$), we have fitted the last two data points together with the one measured last (star in Fig. 9a). It turns out that the line fitted to these points has significantly lower inclination than the previous one (0.941±0.006 vs. 0.980±0.019). The presence of additional absorber, if present, is thus more than compensated by reduction of absorption due to onset of coagulation, which in turn increases epidermal fluence (and thereby heating) and increases the depth of laser heating (Figs. 7a, b).

To analyze the latter effect, we define effective heating depth, $\zeta$, as a normalized weighted sum

$$\zeta = \frac{\sum_i T_i z_i}{\sum_i z_i}. \tag{4}$$

The dependence of $\zeta$ (4) on dual-wavelength radiant exposure in PWS (Fig. 9b) shows that effective heating depth is steadily increasing with $H_0$ from 1.8 to 9 J/cm$^2$ (dashed line). Moreover, on returning to the lowest radiant exposure value, $\zeta$ remains at the highest level reached, confirming irreversibility of the laser-induced transformation.

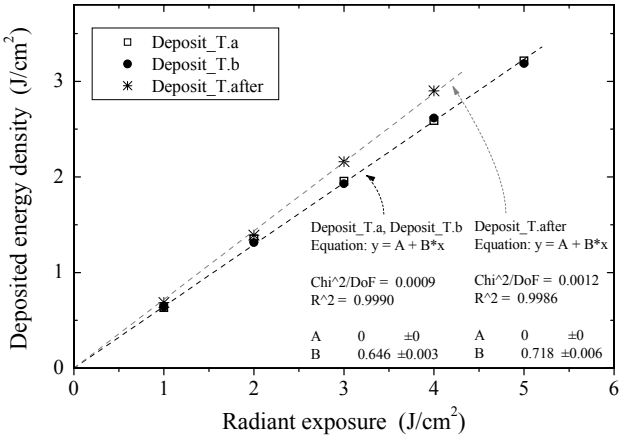


Figure 10: Deposited energy density ε (3) in normal skin as a function of 532 nm radiant exposure. Dashed lines are linear fits to data points corresponding to initial irradiation with increasing radiant exposures (open squares and solid circles) and subsequent irradiation with decreasing radiant exposures (stars).
(volunteer B, dual-wavelength irradiation)

The results obtained from the same analysis on laser-induced profiles in heathy skin (Fig. 8) are somewhat different. Here, as well, the line fitted to the five pairs of $\varepsilon$ values measured when increasing the radiant exposure (open squares and solid circles) differs from the line, fitted to the data points corresponding to the subsequent profile measurements (stars). Unlike in the previous example, however, the efficiency of energy deposition increases upon laser irradiation (from 0.65 to 0.72). This could be attributed to mild erythema or increased dermal scattering, which increase energy uptake in normal skin, while the coagulative effect on larger and deeper vessels in normal dermis is negligible at such low radiant exposures.

## 5. CONCLUSIONS

Pulsed photothermal radiometry is a viable tool for analysis of interaction of PWS with various laser systems. The reconstructed profile shapes reveal modifications of optical properties and analysis of deposited energy density allows reliable detection of irreversible changes inside the lesion. The results indicate that the dual-wavelength laser system with 25 ms pulse duration and visible radiant exposure around 1.5 J/cm$^2$ at 532 (and additional and 2.7 J/cm$^2$ (at 1064 nm) exhibits somewhat higher energy deposition than a customary KTP laser. Results obtained with incrementally increasing radiant exposure toward therapeutic values are inconclusive due to interplay between irreversible changes in absorption and scattering properties of several lesion constituents, which can not be resolved without appropriate modeling.

## ACKNOWLEDGEMENTS

The authors thank Fotona d.d. (Ljubljana, Slovenia) for the loan of the Dualis Tandem laser system and acknowledge technical assistance provided by Drs. Walfre Franco and Wim Verkruysse, and prof. Bernard Choi. This work was supported by the Research Agency of Slovenia (Research Programme Grant P1-0192, Bilateral Collaboration Grant BI-US/05-06/0022, Junior Researcher Grant 3311-03-831066) and the National Institutes of Health (NIH; research grant AR-48458 to JSN). Institutional support from the NIH, Office of Naval Research, and Beckman Laser Institute and Medical Clinic Endowment is also acknowledged.

## REFERENCES

1. S. H. Barsky, S. Rosen, D. E. Geer, and J. M. Noe, "The nature and evolution of port wine stains: a computer-assisted study," *J. Invest. Dermatol.* **74**, pp. 154-157, 1980.
2. J. S. Nelson, T. E. Milner, B. Anvari, B. S. Tanenbaum, S. Kimel, L. O. Svaasand, and S. L. Jacques, "Dynamic epidermal cooling during pulsed laser treatment of port-wine stain. A new methodology with preliminary clinical evaluation," *Arch. Dermatol.* **131**, pp. 695-700, 1995.
3. J. S. Nelson, B. Majaron, and K. M. Kelly, "Active skin cooling in conjunction with laser dermatologic surgery," *Semin. Cutan. Med. Surg.* **19**, pp. 253-266, 2000.
4. I. V. Meglinsky and S. J. Matcher, "The determination of absorption coefficient of skin melanin in visible and NIR spectral region," in: Lasers in Surgery: Advanced Characterization, Theraputics, and Systems X, *Proc. SPIE* **3907**, pp. 143-150, Bellingham, WA, 2000.
5. J. K. Barton, G. Frangineas, H. Pummer, J. F. Black, "Cooperative phenomena in two-pulse, two-color laser photocoagulation of cutaneous blood vessels," *Photochem. Photobiol.* **73**, pp. 642-650, 2001.
6. J. F. Black, N. Wade, J. K. Barton, "Mechanistic comparison of blood undergoing laser photocoagulation at 532 and 1064 nm," *Lasers Surg. Med.* **36**, pp. 155-156, 2005.
7. N. S. Sadick, "Long-term results with a multiple synchronized-pulse 1064 nm Nd:YAG laser for the treatment of leg venulectasias and reticular veins," *Dermatol. Surg*. **27**, pp. 365-369, 2001.
8. N. E. Omura, J. S. Dover, K. A. Arndt, A. N. Kauvar, "Treatment of reticular leg veins with a 1064 nm long-pulsed Nd:YAG laser," *J. Am. Acad. Dermatol.* **48**, pp. 76-81, 2003.
9. U. Ahčan, P. Zorman, D. Recek, S. Ralca, B. Majaron, "Port wine stain treatment with a dual-wavelength Nd:YAG laser and cryogen spray cooling: a pilot study," *Lasers Surg. Med.* **34**, pp. 164-167, 2004.
10. A. C. Tam and B. Sullivan, "Remote sensing applications of pulsed photothermal radiometry," *Appl. Phys. Lett.* **43**, pp. 333-335, 1983.
11. R. E. Imhof, D. J. S. Birch , F. R. Thornley, J. R. Gilchrist, and T. A. Strivens, "Optothermal transient emission radiometry," *J. Phys. E: Sci. Instrum.* **17**, pp. 521-525, 1984.
12. F. H. Long, R. R. Anderson, and T. F. Deutch, "Pulsed photothermal radiometry for depth profiling of layered media," *Appl. Phys. Lett.* **51**, pp. 2076-2078, 1987.
13. R. M. S. Bindra, R. E. Imhof, and G. M. Eccleston, "In vivo opto-thermal measurement of epidermal thickness," *J. De Physique IV* **C7**, pp. 445-448, 1994.
14. S. A. Prahl, I. A. Vitkin, U. Bruggeman, B. C. Wilson, and R. R. Anderson, "Determination of optical properties of turbid media using pulsed photothermal radiometry," *Phys. Med. Biol.* **37**, pp. 1203-1217, 1992.
15. S. L. Jacques, J. S. Nelson, W. H. Wright, and T. E. Milner, "Pulsed photothermal radiometry of port-wine-stain lesions," *Appl. Opt.* **32**, pp. 2439-2446, 1993.
16. T. E. Milner, D. M. Goodman, B. S. Tanenbaum, and J. S. Nelson, "Depth profiling of laser-heated chromophores in biological tissues by pulsed photothermal radiometry," *J. Opt. Soc. Am.* **A 12**, pp. 1479-1488, 1995.
17. T. E. Milner, D. J. Smithies, D. M. Goodman, A. Lau, and J. S. Nelson, "Depth determination of chromophores in human skin by pulsed photothermal radiometry," *Appl. Opt.* **35**, pp. 3379-3385, 1996.
18. S. A. Prahl, "Pulsed photothermal radiometry of inhomogeneous tissue," in: *Progress in Photothermal and Photoacoustic Science and Technology Series: Life and Earth Sciences*, vol. 3, A. Mandelis and P. Hess, eds. (SPIE, Bellingham, 1997).

19. B. Majaron, W. Verkruysse, B. S. Tanenbaum, T. E. Milner, and J. S. Nelson, "Spectral variation of infrared absorption coefficient in pulsed photothermal profiling of biological samples," *Phys. Med. Biol.* **47**, pp. 1929-1946, 2002.
20. B. Majaron and M. Milanič, "Re-evaluation of pulsed photothermal radiometric profiling in samples with spectrally varied infrared absorption coefficient", *Phys. Med. Biol.* **52**, pp. 1089-1101, 2007.
21. M. Milanič, B. Majaron and J. S. Nelson, "Pulsed photothermal temperature profiling of agar tissue phantoms", *Las. Med. Sci.*, 2007 (in press).
22. B. Majaron, M. Milanič, B. Choi, J.S. Nelson, "Selection of optimal infrared detector for pulsed photothermal profiling of vascular lesions," *Proc. SPIE*, **5318**, pp. 121-132, Bellingham, WA, 2004.
23. B. Majaron, M. Milanič, "Effective infrared absorption coefficient for photothermal radiometric measurements in biological tissues," *Laser Surg. Med. Suppl.* **18:**4 (2006)
24. L. O. Svaasand, L. T. Norvang, E. J. Fiskerstrand, E. K. S. Stopps, M. W. Berns, and J. S. Nelson, "Tissue parameters determining the visual appearance of normal skin and port-wine stains," *Lasers Med. Science* **10**, pp. 55-65, 1995.
25. B. Choi, B. Majaron, J.S. Nelson, "Computational model to evaluate port wine stain depth profiling using pulsed photothermal radiometry," *J. Biomed. Opt.* **9**, pp. 299-307, 2004.